Conference Paper, Published Version

Douglas, Steven; Eden, Derek; Simpalean, Adrian; Nistor, Ioan; Cornett, Andrew; Anglin, Dave; Via-Estrem, Lluis; Latham, John-Paul; Xiang, Jiansheng

Experimental Study of Wave-Induced Loading on Breakwater Armour Layers

Coastal Structures 2019 - Nils Goseberg, Torsten Schlurmann (eds) - © 2019 Bundesanstalt für Wasserbau
ISBN 978-3-939230-64-9 (Online) - DOI: 10.18451/978-3-939230-64-9_015

Experimental Study of Wave-Induced Loading on Breakwater Armour Layers

S. Douglas, D. Eden, A. Simpalean, T. Kozlowski & I. Nistor
University of Ottawa, Ottawa, Canada

A. Cornett
National Research Council of Canada, Ottawa, Canada

D. Anglin
W.F. Baird & Associates Coastal Engineers Ltd., Ottawa, Canada

L. Via-Estrem, J. P. Latham, J. Xiang
Imperial College of London, London, U.K.

Abstract: A series of experimental tests were conducted in a wave flume at the National Research Council of Canada to study the hydrodynamics of breakwater armour layers. Wave-induced loads were measured on an individual concrete armour unit embedded in a full single-layer armoured breakwater. An image processing technique was applied to video footage recorded during each test to extract time-histories of water surface elevation at various locations on the structure in addition to time-histories of runup/rundown elevation. A qualitative analysis of the behaviour of the slope-normal and slope-parallel force signals is given in relation to the results obtained from the image processing. Analysis of the data revealed a strong positive correlative relationship between wave period and maximum slope-parallel forces acting towards the structure toe as well as maximum slope-normal forces acting towards the structure interior. The influence of wave period and breaking wave type on the dynamic relationship between these two force components is discussed in detail.

Keywords: Breakwater, rubble mound, armour unit, hydrodynamic force, wave load, image processing

1 Introduction

The economic design of a rubble mound breakwater is a delicate balance between cost and uncertainty. A significant portion of the overall design effort is afforded to selecting an armour unit massive enough to resist wave-induced loads while remaining economically feasible to construct. Failure of a single armour unit occurs when the destabilizing forces exceed the stabilizing forces, causing it to be dislocated from the array of other armour units it is embedded within. A reasonable approach to this optimization problem would be based on a balance of these forces, as is the case for the majority of other man-made static structures. However, due to the extremely complex flow of waves through the armour layer, direct assessment of the wave-induced forces on individual armour units has been difficult (Hald, 1998). The greater part of research performed to find a solution to this problem has avoided an approach based on understanding the physical mechanisms underlying the development of forces on these structures (Medina and Gómez-Martín, 2012). Rather, empirically derived formulae that relate sea-state and structural variables to the hydraulic stability of armour units have been the favoured approach. The most notable of which, commonly used in modern design practice, are those of Hudson (1958) and Van der Meer (1988). Although these methods may be sufficient for a number of applications, for others, the inherent uncertainty may pose too great a risk.

In relatively recent developments, some steps have been taken towards enhancing our understanding of the hydrodynamics of breakwater armour layers. Tørum (1994) performed a series of experimental tests whereby force was measured on an individual stone embedded in the main armour layer of a berm breakwater. Simultaneous velocity measurements were taken at a location just above the force-measuring device. With these data, the authors were able to approximate the drag and inertia coefficients for use in the Morison force formulation. Further investigations were performed by Moghim and Tørum (2012) to study wave-induced forces on stones in a berm breakwater before and

after structural reshaping for various armour stone locations with respect to still water level. Their measurements of wave-induced forces on individual armour stones in a berm breakwater before structural reshaping suggest that the largest forces occur above still water, with the largest of the slope-normal component acting into the structure and the largest of the slope-parallel force acting up the slope.

Although their study did not include direct measurement of the forces acting on individual stones, Jensen et al. (2014) performed detailed measurements of pressure gradients and velocity fields occurring in a breakwater when subjected to waves. Their measurements were used to extrapolate hypothetical pressure-induced forces on individual stones beneath the main armour and shear stresses acting on the main armour layer. Analysis of the time-series showed that maximum outward-directed pressure gradients occur at or just below the location of maximum rundown at the time of maximum rundown. From their LDA (Laser Doppler Anemometry) velocity measurements performed at similar locations, they suggest that maximum shear stress exerted on the main armour layer is connected to the event producing the maximum outward-directed pressure gradients. The results and discussion presented by Jensen et al. (2014) appear to be in agreement with several conclusion made by Hald (1998), who performed a series of experiments to relate wave-induced forces on armour units to incident wave characteristics.

Owing to their inherent economic efficiency, significant effort has been devoted to the research of berm breakwaters, of which some of the abovementioned works serve as pertinent examples. Berm breakwaters often require a smaller average stone size with a wider gradation compared to their single- or two-layer armoured breakwater relatives. In berm breakwaters, stones of varying size are placed at random to form the main armour layer. As such, each stone, embedded within the layer, is exposed to wave-induced flow in a, somewhat, arbitrary way. To further complicate matters, berm breakwaters are designed to allow for reshaping. In this way, the profile of the structure reshapes itself under the influence of wave action until it comes to a natural equilibrium that increases stability. In some regions of the world, the quantities or sizes of natural stone needed for a berm breakwater may not be available. For regions where quantities or size of natural stone is not a limiting factor, strict requirements may be imposed (owing to its structural function or limited space, for example) that necessitate the use of a structure that remains statically stable over its design life.

In these circumstances, single-layer armoured breakwaters can be an economically-viable solution. In single-layer systems, resting positions of armour units are closely monitored during construction to ensure that they are within an acceptable distance from the placement grid developed during the design. Single-layer (and some two-layer) systems are built using concrete armour units designed for little to no damage and, so, the designer has greater confidence that the hydrodynamic conditions occuring on (and within) the breakwater, accounted for in the design, will closely mirror that of the prototype structure. It stands to reason, then, that the design of single-layer systems ought to yield the greatest benefit from having an in-depth knowledge of the hydrodynamics occurring within breakwaters.

The measurements and analysis thereof presented in this work focus on results obtained with an instrumented armour unit (IAU) installed at single location below the still water line (labelled L0, as shown in Fig. 1-(a)), corresponding, approximately, to the location of maximum rundown on the structure. In the discussion of results, particular emphasis is given to describing the influence of wave period on the dynamic relation between slope-parallel and slope-normal forces.

2 Physical model

The experiments were conducted at the National Research Council of Canada, Ottawa, Canada, in a steel wave flume, fitted with glass side walls, measuring $60m$-long x $1.2m$-wide x $1.2m$-high. A hydraulically powered wave machine equipped with an active wave absorption system, located at the north end of the flume, was used to generate regular waves with wave height, H = 0.20m, and wave periods T = 1.4, 2.0, and 2.4s. A precise model scale cannot be defined for these experiments, as the model structure was not intended to represent a specific prototype structure. However, comparing the wave conditions and characteristic length (c) of the armour unit used in the current study with that of past engineering investigations, the model scale employed for the current work is estimated to be on the order of 1:15 – 1:25.

2.1 *Model configuration*

The waves, generated at the north end of flume, propagate through a water depth of $0.72m$ until arriving at the toe of the bathymetry, located at $x = 31.31m$ (Fig. 1-(a)). At this point, the bottom of the flume increases in elevation with a mild slope, $\alpha = 2.4\%$, until it meets the toe of the structure, located at an elevation of $0.22m$. The substructure, upon which armour units were placed, was constructed from a continuous sheet of polyvinyl chloride (PVC), fastened to a rigid stainless steel frame. A rubberized coating was applied to the seaward facing side of the substructure to provide additional roughness and to help maintain initial armour unit positions during construction. A placement grid, designed to achieve a standard armour layer packing density coefficient $\phi = 0.62$, was painted on top of the substructure and was used to guide the placement of each armour unit.

A total of 162 Core-Loc™ armour units were cast from mortar, using a set of plaster molds created from a single 3D-printed Core-Loc. The model breakwater slope was used to support a 8/9 units-wide x 19 units-high armour layer. The toe row was placed at the front of the structure in standard cannon formation, as used in practice. Subsequent rows were placed on the slope above the toe using the placement grid as a guide to achieve the target packing density. In addition to using the placement grid for the centroid locations, care was taken to ensure that each unit was placed according to the following placement rules (summarized by Muttray et al., 2005), as prescribed by the Core-Loc manufacturers, Concrete Layer Innovations (CLI);

- Each unit shall make at least one point of contact with the underlayer and make contact with two units in the row below, locking them in place;
- Units residing within the same row shall not make contact with each other; and
- Armour units shall not have the same orientation as those immediately adjacent in the same row.

Since the primary focus of this work is to study the effect of various sea-state and structural variables on hydrodynamic quantities (e.g., wave-induced forces, pore pressure, etc.) before instability occurs, armour units were fixed in place by injecting a small bead of silicon at all points of contact with the underlayer and adjacent units.

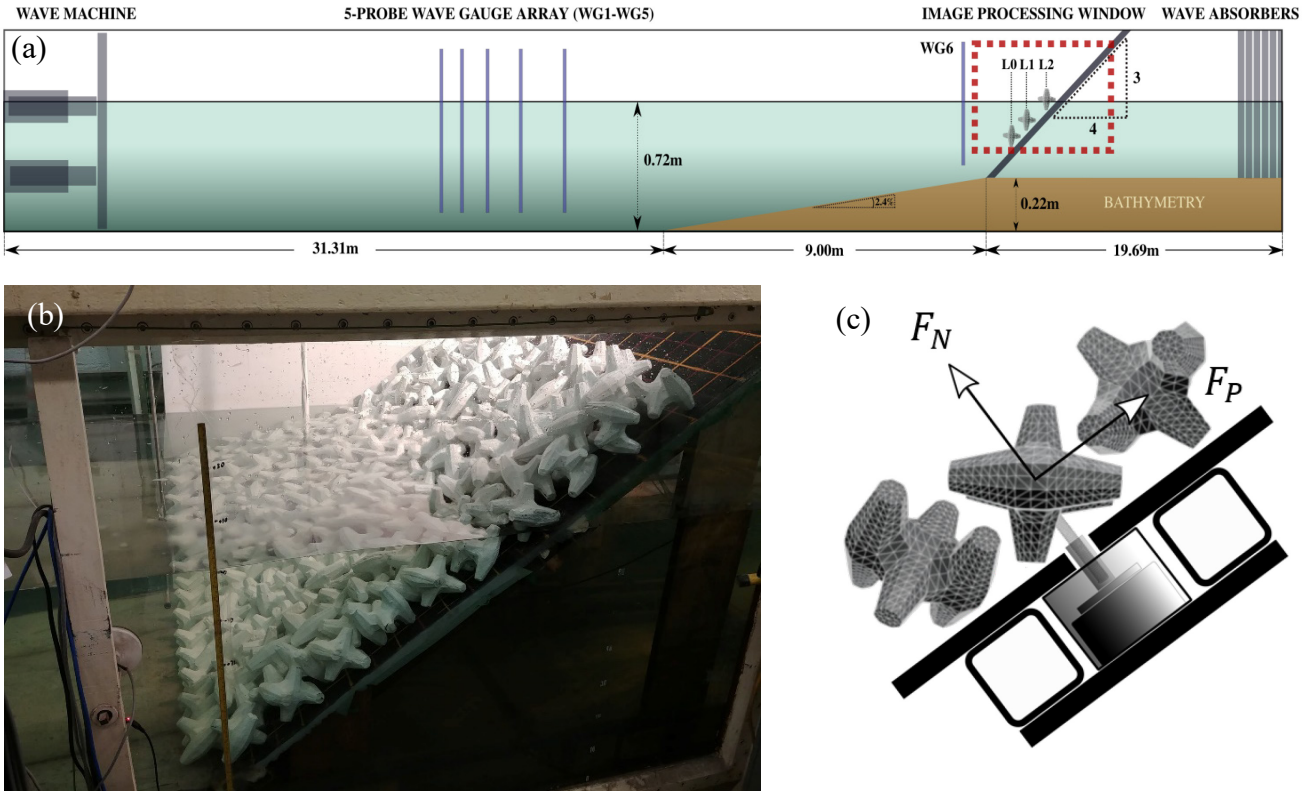

Fig. 1. (a) Illustration of the physical model configuration; (b) Photograph of the tested structure and; (c) Schematic of the armour unit-force sensor coupling mechanism and coordinate system.

Wave-induced forces were measured on a single armour unit (herein referred to as the Instrumented Armour Unit, IAU) residing within the layer by supporting a 3D-printed Core-Loc on a six-axis force sensor (ATI Mini45) mounted to two steel structural members on the underside of the substructure. Care was taken to ensure that the IAU did not contact any of the surrounding units or the surface of the PVC substructure. The force sensor was located in a waterproof housing to ensure that no water flowed through substructure, creating undesired spurious forces. A schematic of the armour unit-force sensor mounting arrangement, as well as the coordinate system, referred to herein, is shown in Fig. 1-(c). A photograph of the completed armour layer, prior to testing, is given in Fig. 1-(b). The force signals were re-zeroed in calm water before each test, when the IAU was fully submerged, effectively removing both gravitational and buoyancy forces.

2.2 Wave conditions

Drive signals for the wave machine were calibrated for a wide range of wave periods with a target wave height of H = 0.20m at the toe of structure. Calibration of these signals was performed without the interference of the structure, thereby removing any potential error in the measured wave height introduced in the process of separating incident and reflected waves. A series of mechanical wave absorbers were placed at the opposing end to the wave machine in order to minimize the amount of reflection. Using a five-probe array of wave gauges located just offshore from the toe of the bathymetry, collected time-series were analysed to separate incident and reflected wave signals to confirm reflected wave energy was less than 1% that of the incident. Wave characteristics at a point coinciding with the location of the toe of the future structure were extracted from the water surface elevation time-series collected from a single capacitance-type wave gauge (WG6). For each drive signal, the gain factor was adjusted until the measured wave height was within 1% of the target wave height. A continuous video record of wave interaction with the model breakwater was recorded through the glass side wall of the flume for the full duration of every test. Three frames extracted from video footage for selected tests are shown in Fig. 2-(a) to Fig. 2-(c), and illustrate the different breaking wave types (i.e, plunging, spilling, and surging, respectively).

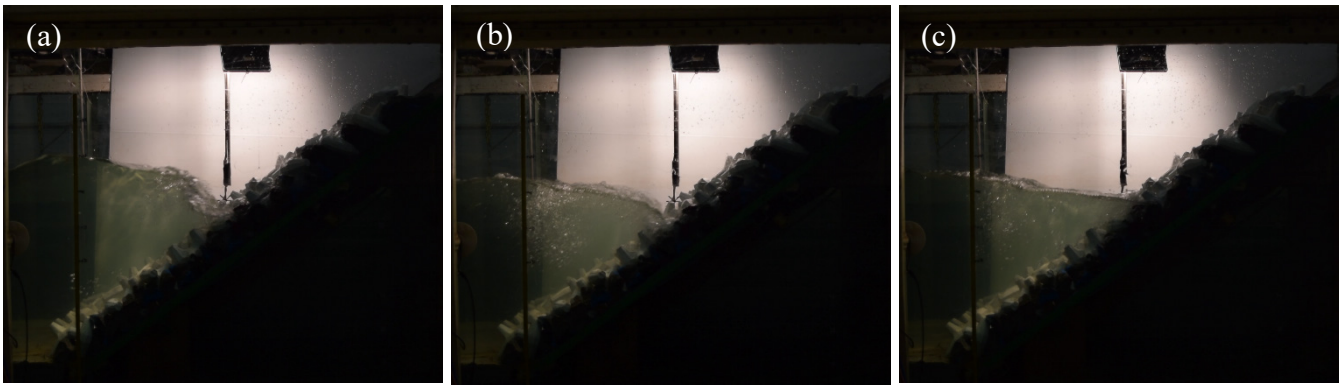

Fig. 2. Frames from the video footage captured of waves (wave height, H = 0.20m) arriving at the structure for wave periods (a) T = 1.4s; (b) T = 2.0s and; (c) T = 2.4s.

2.3 Image processing

A non-intrusive image processing technique was developed to obtain water surface elevation time-series, runup profiles, maximum runup and rundown elevations, and runup velocities and accelerations on the structure. In the sample images shown in Fig. 3, a translucent light blue colour overlay has been applied to areas, determined by the algorithm, to be both above the structure and below the water surface. These areas are found by converting the original RGB frames to HSV and applying a threshold filter on a range of hue values found nowhere else in the images except for in the region of interest. By taking the highest pixel determined to be below the water surface in any given column of pixels, it was possible to convert its location in the image (column, row) to a physical location (x, z) by means of a calibration coefficient.

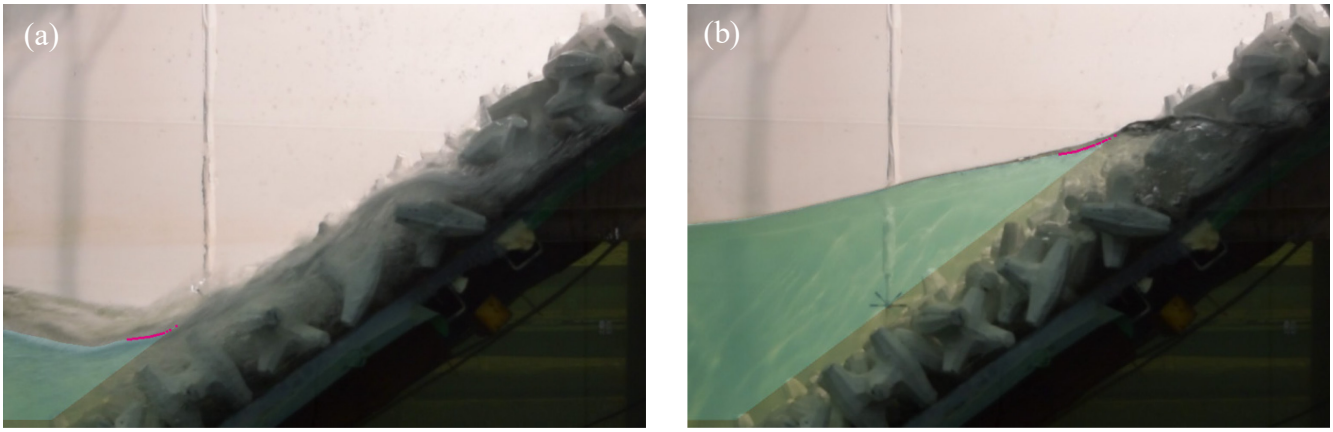

Fig. 3. Sample visualizations of the image processing technique used to find water surface elevations, runup/rundown elevation, and runup velocity on the structure at times corresponding to maximum rundown (a) and runup (b).

The series of pink pixels seen in Fig. 3, which span a short distance along the water surface where it intersects the structure, were used to calculate runup and rundown velocities and accelerations, as well as estimate a time-series of runup elevation. The algorithm determines the location of these points by applying the same threshold technique described above, except, only in a single line of pixels (each one, slightly further away from the structure than the last) that run parallel to the surface of the structure. Each pink pixel represents the point where the inclined line of pixels intersects the water surface. The average change in location of the pixels between consecutive frames was calculated to produce a smooth time-series of runup velocity. By using only the pink pixel closest to the structure, a time-series of runup elevation was constructed (with its maximums and minimums representing maximum runup and rundown, respectively).

3 Discussion of results

3.1 Qualitative analysis of wave-induced forces

The normalized slope-parallel and slope-normal forces (see Fig. 1-(c) for definition) are provided in Fig. 4-(a) and Fig. 4-(b), respectively, for wave periods T = 1.4s (Fig. 4-(i)), 2.0s (Fig. 4-(ii)), and 2.4s (Fig. 4-(iii)). In this figure, the slope-parallel and slope-normal forces are normalized with their respective directional component of the IAU's submerged weight (assuming concrete with density ρ = 2400 kg/m^3) available to resist that force (i.e., $W_{parallel}$ and W_{normal}, respectively). It should be noted that no correction for the reduction in buoyancy force that occurs when the unit becomes only partially submerged has been applied. The discussion that follows is intended as a qualitative analysis of the behavior of the normalized forces acting on the IAU with respect to the water surface elevation above the IAU, shown as a red dotted line, and runup elevation (i.e., vertical location of the leading edge of the wave on the surface of the structure), shown as a grey dashed line. Units of the latter two variables have been normalized with the characteristic length, c = 0.12m, of the Core-Loc units.

In Fig. 4-(a)(i), the minimum slope-parallel force (i.e., maximum slope-parallel force acting down the slope) occurs during the rundown phase, just before the halfway point between the time of maximum wave runup and maximum rundown. The slope-parallel force begins to rise from its minimum value before the rundown reaches its lowest point on the structure. If the minimum rundown elevation was below the lowest point of the IAU, one would expect the slope-parallel force to continue to decline as the volume of water rushing down the structure continued to accelerate under the influence of gravity. However, we can see in Fig. 4-(a)(i) that this is not the case for wave period T = 1.4s. During the rundown, the time-series of water surface elevation above the IAU (red dotted line) is interrupted, indicating that the water surface elevation has passed below the highest point of the IAU. However, following the runup elevation time-series, the difference between the highest point of the IAU and maximum rundown is significantly less than 1.0 (approximately, 0.2), with a difference of greater than 1 representing a case for which the maximum rundown elevation is lower than the lowest point of the IAU. Since the water surface elevation at maximum rundown elevation

bisects the IAU, the increase in slope-parallel force, from its minimum value, occurring before maximum rundown can be explained by the gradual build-up of water flowing out of the structure at the front of the IAU. The slope-parallel force makes a gradual transition from negative to positive at around the time of maximum rundown. After this transition, a markedly steep increase in slope-parallel force is observed, beginning at the time of maximum rundown and ending at the time where the IAU becomes fully submerged (i.e., where the red dotted line segments begin), where the maximum slope-parallel force is observed. After the leading edge of the wave passes the IAU, slope-parallel forces decline rapidly, crossing zero at, approximately, the time at which water surface elevation above the IAU is at a maximum.

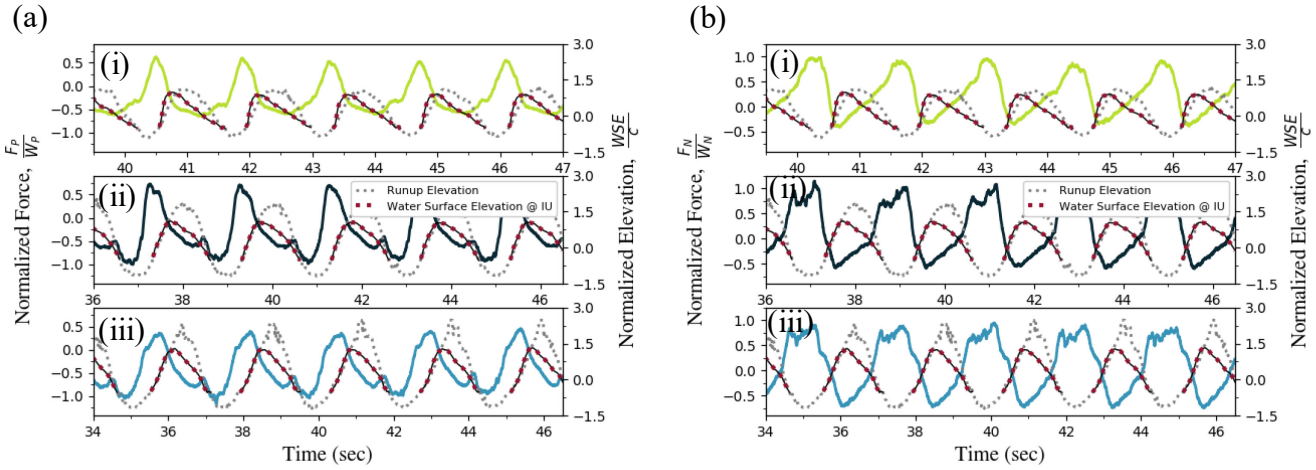

Fig. 4. Comparison of the slope-parallel (a) and slope-normal (b) normalized force acting on the IAU with respect to runup elevation (dotted grey line) and water surface elevation above of the IAU (dark red dotted line) for wave periods (i) T = 1.4s; (ii) T = 2.0s and; (iii) T = 2.4s.

A similar case in the behavior of the slope-parallel force signal is observed for the collapsing (T = 2.0s) and surging (T = 2.4s) breakers, shown in Fig.4-(a)(ii) and Fig. 4-(a)(iii), respectively. In contrast to the case of the plunging (T = 1.4s) breaker, slope-parallel forces acting on the IAU continue to decline from their maximum until maximum rundown. This difference in behavior of the slope-parallel force signal is attributed to the difference in location of maximum rundown elevation with respect to elevation of the IAU. In Fig. 4-(a)(ii) and Fig. 4-(a)(iii), the difference between maximum normalized rundown elevation and the highest point of the IAU is equal to or greater than 1.0, indicating that the IAU is fully exposed to the accelerating downrush of water when rundown is at its maximum (visualized in Fig. 3-(a)). As is the case for the two longer wave periods considered here (i.e., T = 2.0 and 2.4s), the slope-parallel forces continue to decline for a greater portion of the wave cycle in comparison to T = 1.4s, producing significantly larger forces acting towards the toe of the structure during rundown.

For all three wave periods considered here, the maximum slope-parallel force is observed at, approximately, the time at which the depth of water above the IAU becomes greater than zero at the beginning of the runup phase. In all three cases, the IAU experiences positive slope-parallel forces for only a small portion of the full wave cycle. In comparison to the minimum slope-parallel forces, seen in Fig. 4-(a), the magnitude of the maximum slope-parallel forces bear weaker correlation to wave period. For the two shorter wave periods, T = 1.4 and 2.0s, the maximum slope-parallel forces reach, roughly, 60-70% of the submerged weight of the IAU available to resist that force in the slope-parallel direction. In the case of the longest wave period, T = 2.4s, maximum slope-parallel forces reach, approximately, 45% of the IAUs submerged weight. The authors surmise that the differences in maximum slope-parallel forces observed for the two smaller wave periods and the largest wave period is linked to the nature of the leading edge of the wave. In the case of the former, the wave breaking process has started before arriving at the IAU, producing large flow accelerations and velocities in the volume of water that submerges the unit at the beginning of the runup phase, thereby creating the comparatively larger forces seen in Fig. 4-(a)(i) and Fig. 4-(a)(ii).

Normalized slope-normal forces acting on the IAU are given in Fig. 4-(b) for the three wave periods considered. The first feature of these force signals, distinguishing them from the slope-parallel forces, is the length of time spent at near-maximum magnitude. For the slope-parallel forces, a maximum occurs shortly after the minimum and quickly diminishes thereafter. On the other hand, the

slope-normal forces reach a maximum at, approximately, the same time at which the depth of water above the unit reaches zero (during the rundown) and remains near this maximum until water depth above the IAU becomes greater than zero (during the runup). From the three slope-normal force signals given in Fig. 4-(b), no clear correlation can be noted between maximum slope-normal force and wave period. Over the next quarter of a wave cycle, slope-normal forces decline at a relatively constant rate until the wave crest is directly above the IAU (i.e., water depth above the IAU is at a maximum), at which time the minimum slope-normal force is observed. Unlike the maximum slope-normal force, a strong positive correlation is noted between wave period and minimum slope-normal force (i.e., larger wave periods produce larger forces into the slope).

3.2 Relationship between slope-parallel and slope-normal forces

In Fig. 5, a normalized force hodograph (Fig. 5-(b)) is shown for a selected portion of the full signal (Fig. 5-(a)) with a length equivalent to five wave cycles. Following the closed loops, one for each wave period, shown in Fig. 5-(b), in a clockwise direction, we can see how the relationship between slope-parallel and slope-normal forces acting on the IAU changes over the duration a wave cycle. The separation distance between lines contained in the same loop (i.e., belonging to the set of lines for that wave period) is indicative of the variability of forces at that point in the wave cycle. Additionally, by plotting the hodograph for different values of wave period, evidence of the effect (and its strength) of wave period can be made visible in a convenient format.

From Fig. 5-(b), it can be seen that as wave period increases from the smallest value considered (i.e., T = 1.4s), slope-normal forces go from dominantly positive to distributed relatively equally in both positive and negative directions. This is primarily achieved through significant increases to slope-normal forces acting into the structure with increases in wave period. For all three cases, in general, maximum and minimum slope-normal forces occur when slope-parallel forces are less than 50% of their maximum (i.e., when rundown is at maximum and when the wave crest is directly above the IAU, respectively). In Fig. 5-(b), it is noted that for the longest wave period considered that particularly large negative slope-normal forces (into the structure) are accompanied with large negative slope-parallel forces (down the slope).

Slope-parallel forces, for the plunging and collapsing (T = 1.4 and 2.0s, respectively) breakers are distributed relatively equally in negative and positive directions. For the surging wave (T = 2.4s), however, a distinct change in its distribution of slope-parallel forces is observed. The slope-parallel forces for this case act predominantly towards the toe of the structure, with a maximum magnitude roughly 75% greater than that for the plunging breaker.

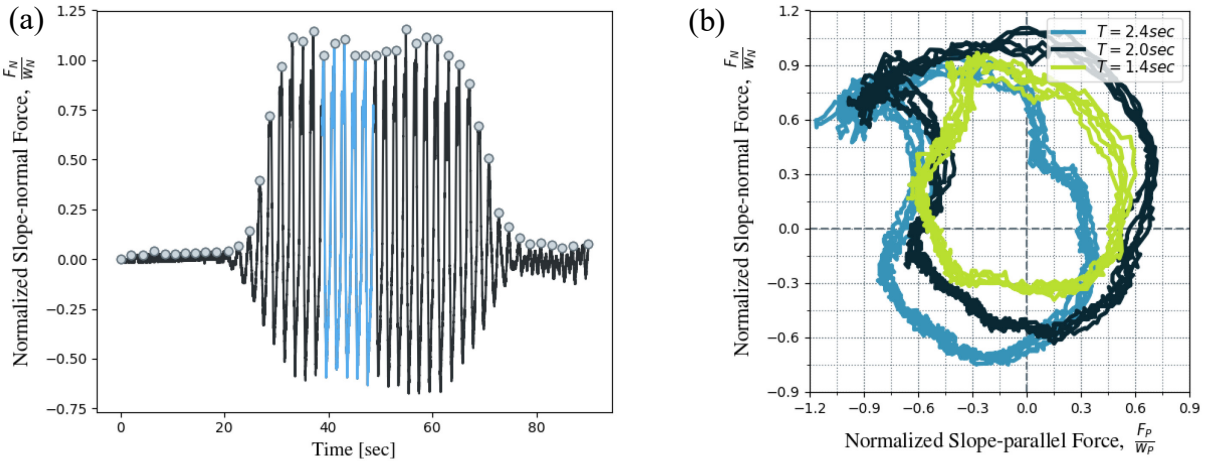

Fig. 5. (a) Full time-history of normalized slope-normal force (dark blue) with five wave cycles selected for analysis (light blue) and (b) Normalized force hodograph for wave periods T = 1.4s, 2.0s, and 2.4s.

Given that positive slope-normal and slope-parallel forces acting on the IAU work against the stabilizing forces derived from its weight, the further the hodograph extends (away from the origin) in the first quadrant (top-right) of Fig. 5-(b), the greater the risk of being dislocated from the armour layer. For the longest wave period considered, T = 2.4s, the time at which the IAU would be most vulnerable to being ejected from the armour layer is, likely, around the time that slope-parallel forces

are near zero and slope-normal forces are near their maximum. Although larger slope-normal forces than those occurring when slope-parallel forces are near zero can be seen in Fig. 5-(b), the authors believe that the larger negative slope-parallel forces occurring at that time would counteract the small decrease in stability afforded by the relatively smaller change in slope-normal forces. For the two shorter wave periods considered, T = 1.4 and 2.0s, the point at which the IAU would be most vulnerable to ejection likely occurs at the point in the wave cycle when slope-parallel forces are, approximately, 50% of their maximum positive value when slope-normal forces are near their maximum (point in the wave cycle furthest away from the origin in the first quadrant). Although the ratio of the slope-parallel to slope-normal forces at the time the IAU is most vulnerable to dislocation differ amongst the three periods considered, it is observed at the same point in the wave cycle for each case. In particular, the point at which the IAU was at greatest risk of being ejected from the armour layer was noted to occur, approximately, at the point in the wave cycle where the IAU becomes fully submerged during the runup phase, shortly after maximum rundown is observed.

4 Conclusions

This paper presents results of the section of a wider experimental program dealing with wave loading on breakwater armour units. This portion of the study details the results of an image processing algorithm, developed by the authors, and analysis of the hydrodynamic-induced loading on an individual unit located at, approximately, maximum rundown elevation. Several conclusions are drawn from the present work and can be summarized as follows:

- From the discussion presented in Section 3.1, the authors expect the largest slope-parallel forces acting towards the toe to occur on armour units residing in the first row of armour units entirely above the elevation of maximum rundown;
- The force signals shown in Fig. 4-(a) indicate that the magnitude of the maximum slope-parallel force acting towards the toe is positively correlated to wave period, with larger waves periods producing larger forces down the slope;
- The magnitude of the maximum slope-parallel force acting upslope towards the crest of the structure appears to have weakly negative to zero correlation to wave period, with changes in wave period having little to no discernable effect on forces acting upslope;
- From Fig. 4-(b) and Fig. 5-(b), maximum slope-normal forces appear to have little to no correlation to wave period, with all three wave periods considered producing similar maximum forces directed outward from the interior of the structure.
- From Fig. 4-(b), it can be seen that for all three wave periods, maximum slope-normal forces occur at the time of maximum rundown;
- Fig. 5-(b) indicates strong positive correlation between wave period and maximum negative slope-normal forces, with large wave periods producing large forces directed into the slope;
- For all three wave periods, it is noted in Fig. 4-(b) that the greatest negative slope-normal forces (acting into the slope, toward the structures interior) occur when water depth above the armour unit is at a maximum (i.e., when the wave crest is directly overhead); and
- For all three wave periods considered, the conditions where the IAU was considered to be most vulnerable to dislocation were observed shortly after maximum rundown, at the moment the IAU became fully submerged by the incoming wave.

Acknowledgements

The authors are grateful for the support of the Natural Sciences and Engineering Research Council through the NSERC-CRD Grant held by Prof. Ioan Nistor (No. 211367), in collaboration with Baird & Associates and the NSERC-PGSD held by the lead author. The authors also extend their thanks to the National Research Council of Canada (NRC-OCRE) for both their technical and financial support towards the experimental program.

References

Hald, T. (1998) Wave induced loading and stability of rubble mound breakwaters. PhD Thesis. Hydraulics & Coastal Engineering Laboratory, Department of Civil Engineering, Aalborg University, Denmark; 1998.

Hudson, R.Y. (1958). Design of quarry stone cover layer for rubble mound breakwaters. Research Report No. 2-2. Waterways Experiment Station, Coastal Engineering Research Centre, Vicksburg, USA.

Jensen, B., Christensen, E.D., Sumer, B.M. (2014). Pressure-induced forces and shear stresses on rubble mound breakwater armour layers in regular waves. Coast Eng. 91,60–75.

Medina, J.R. and Gómez-Martín, M.E. (2012). K_D and safety factors of concrete armor units. Proceedings of the 33rd International Conference on Coastal Engineering, Santander, Spain, 2012.

Moghim, M. N., and Tørum, A. (2012). Wave induced loading of the reshaping rubble mound breakwaters. Applied Ocean Research, 37, 90–97.

Muttray, M., Reedijk, J., Vos-Rovers, I., Bakker, P. (2005). Placement and structural strength of Xbloc® and other single layer armour units, ICE Coasts, Marine Structures and Breakwaters, September 2005, Edinburgh.

Tørum, A. (1994). Wave induced forces on an armour unit on a berm breakwater. Journal of Waterway, Port, Coastal and Ocean Engineering, American Society of Civil Engineers;120(3).

Van der Meer, J.W. (1988). Rock slopes and gravel beaches under wave attack. Ph.D. Thesis, Delft University of Technology, Delft, the Netherlands.

Van Gent, M. (1995). Wave interaction with permeable coastal structures. PhD Thesis. Delft University of Technology, The Netherlands, December 1995.